Title

Repair of DNA breaks is imprecise and biased towards joining of incompatible DNA ends in chronic lymphocytic leukemia

Authors

[1,2,4]Franz Josef Gassner, [1,2,4]Maria Schubert, [1,2,4]Stefan Rebhandl, [1,2]Karina Spandl, [1,2]Nadja Zaborsky, [1,2]Kemal Catakovic, [1,2]Stephanie Blaimer, [3]Daniel Hebenstreit, [1,2]Richard Greil, [1,2,5]Roland Geisberger

Running title

Repair of DNA breaks in chronic lymphocytic leukemia

Key words

CLL, NHEJ, MMEJ, DNA repair

Financial support

This work was supported by the SCRI-LIMCR, the Province of Salzburg, the City of Salzburg and grants from the Austrian Science Fund FWF to R.Ge. (FWF; P24619 and P28201).

Affiliation

[1]Department of Internal Medicine III with Haematology, Medical Oncology, Haemostaseology, Infectious Disease, Rheumatology, Oncologic Center, Laboratory for Immunological and Molecular Cancer Research, Paracelsus Medical University Salzburg, Austria

[2]Cancer Cluster Salzburg, Austria

[3]School of Life Sciences, University of Warwick

[4]equally contributing

[5]correspondence and material requests:

Roland Geisberger

Laboratory for Immunological and Molecular Cancer Research, Paracelsus Medical University Salzburg

Müllner Hauptstr 48

5020 Salzburg, AUSTRIA

r.geisberger@salk.at

Tel: 0043 57255 25847

Fax: 0043 57255 25998

Conflict of interests

The authors declare no potential conflicts of interest

word count: 5660; total number of figures: 6; tables: 0

Abstract

Cancer is a genetic disease caused by mutations and chromosomal abnormalities which contribute to uncontrolled cell growth. In addition, cancer cells can rapidly respond to therapies by accumulating novel genetic lesions to gain drug resistance and develop relapsing disease. In particular, in chronic lymphocytic leukemia (CLL) diverse chromosomal aberrations have been found. Improper repair of DNA double strand breaks (DSBs) is a major source for genomic abnormalities. In this study, we examined the repair of DNA DSBs by non-homologous end joining in CLL by performing plasmid based repair assays in primary CLL cells and normal B cells as well as TALEN/Cas9 induced chromosomal deletions in the CLL cell line Mec1. We show that repair of DNA is aberrant in CLL cells, featuring perturbed DNA break structure preference with efficient joining of non-cohesive ends and more deletions at repair junctions. In addition, we observed increased microhomology-mediated end joining (MMEJ) of DNA substrates in CLL together with increased expression of MMEJ specific repair factors. Our results implicate an inherently aberrant DNA DSB repair in the acquisition of subclonal genomic structural variations important for clonal evolution and treatment resistance in CLL.

Implication

This study shows that compared to normal B cells, CLL cells have an aberrant DNA ligase expression profile, which leads to imprecise and promiscuous DNA end joining likely increasing susceptibility for the acquisition of chromosomal aberrations.

Introduction

Whole genome sequencing revealed the presence of numerous clonal and subclonal somatic mutations as well as somatic rearrangements in cancer genomes(1-3). Upon cancer therapy, subclonal refractory cells harboring acquired novel chromosomal aberrations or gene mutations can expand and may thus contribute to therapy resistance and disease relapse(4-6). A major source for chromosomal rearrangements are DNA double strand breaks (DSBs). DSBs occur constantly during the lifetime of any cell and are normally repaired. However, aberrant repair of DSBs can lead to mis-joining of distant DNA ends, generating deletions, inversions or complex rearrangements of chromosomes(7;8). DSBs are repaired by two major pathways, which are homologous recombination (HR) and non-homologous end joining (NHEJ). HR utilizes the sister chromatide as template for repairing DSBs and is thus primarily confined to S/G2/M phase of the cell cycle, whereas NHEJ simply rejoins two DNA ends and, hence, is the main repair pathway for G1 or G0 arrested cells(7). For NHEJ, a classical and an alternative pathway are described, termed c-NHEJ and a-NHEJ, respectively. While c-NHEJ is dependent on recognition of DNA ends by XRCC5, XRCC6 and DNA-PKc and ligation by DNA Ligase 4 (Lig4)/XRCC4, a-NHEJ is carried out independently of Lig4 and can probably be executed by a diverse set of factors, including different DNA polymerases (δ, θ), DNA nucleases (ERCC1-XPF) and ligases (Lig1, Lig3/XRCC1)(9-11). As a-NHEJ is frequently associated with short microhomologies (MH) at the site of DNA junctions, a-NHEJ is also termed MH mediated end joining (MMEJ).

Chronic lymphocytic leukemia (CLL) is a B cell malignancy characterized by the progressive accumulation of clonal B cells in peripheral blood and lymph nodes. Clinically, the mutation status of the B cell receptor divides patients into subgroups with poor (CLL with unmutated BCR, CLL-UM) and more favorable prognosis (CLL with mutated BCR, CLL-Mut)(12-14). While

many of the hematological malignancies show typical entity-specific chromosomal abnormalities(15), there is no specific aberration defining CLL. Instead, in addition to more common chromosomal abnormalities like del(17p), del(11q), del(13q) and Tri12, conventional cytogenetics as well as novel whole genome sequencing approaches revealed a complex set of different chromsomal aberrations in CLL, with CLL-UM samples showing a slight increase in the number of aberrations(3;5;6;16-19).

In this study, we asked whether the frequent occurrence of chromosomal abnormalities is associated with an inherently aberrant DNA DSB repair in CLL. To test this, we analysed DNA DSB repair in primary CLL cells compared to B cells from healthy controls by assessing in vivo repair of artificial DNA substrates carrying diverse DNA break structures using next generation sequencing of repair junctions. These results were corroborated by analyzing the induction of a large chromosomal deletion using TALEN (Transcription activator-like effector nuclease)/Cas9 (Clustered Regularly Interspaced Short Palindromic Repeats associated protein 9) endonucleases (20). Our data show that DNA end joining is less precise and more promiscuous in CLL with a bias towards microhomologies as well as towards joining of incompatible DNA ends, likely due to increased expression levels of Lig1 and XRCC1.

Materials and Methods

Preparation of plasmid repair substrates and transfection of cells.

Plasmids were generated by cloning synthesized inserts (MWG eurofins) into pAX plasmids (sequence shown in supplementary Fig S1). Plasmids were linearized using the respective restriction enzymes (Fermentas), gel purified (Qiagen) and transfected into 293 cells (genejuice, Novagen) and primary B and CLL cells using nucleofection (Amaxa, Lonza). 72h post transfection, cells were harvested and DNA was isolated (Qiagen). Repaired substrates

were PCR amplified using high fidelity Phusion polymerase (Biozym) and tagged 3AOX/5AOX primers (3AOX 5'-GCA AAT GGC ATT CTG ACA TCC-3'; 5AOX 5'-GAC TGG TTC CAA TTG ACA AGC-3'). PCR products were pooled and sequenced on the miseq platform (Illumina). pmCherry was generated by cloning the PCR amplified coding region of mCherry (RG1081 5'-CGCGGGCCCGGGATCGCCACCATGGTGAGCAAGGGCGAGG-3' and RG1082 5'-TCTAGAGTCGCGGCC TACTTGTACAGCTCGTCC-3') into BamHI/NotI digested pEGFP-N1 (clontech) using In-Fusion HD cloning (Clontech). Plasmids pGFP-1 and pGFP-2 were generated by introducing a BsmBI or an EcoRV site at position nt 137 and nt 141 of the GFP coding region using PCR-based mutagenesis of the pEGFP-N1 plasmid. Plasmids were digested using BsmBI/MfeI (pGFP-1) and EcoRV/PstI (pGFP-2) and gel extracted prior transfection together with pmCherry into 293 cells using genejuice transfection reagent or nucleofection (Amaxa) as indicated. 6h before transfection, cells were incubated with highly specific inhibitors for Lig1/3 (L67), DNA-PKc (NU7441) and PARP (Olaparib, all from Selleckchem). After transfection, cells were incubated for further 2 days in presence of inhibitors prior analysis for mCherry/GFP expression using flow cytometry (FC500, Beckman Coulter).

Gene expression analysis

RNA was isolated from purified CLL samples and B cells from healthy controls using high pure RNA isolation kit including DNase digestion (Roche). The same CLL samples as used for plasmid repair assays was used for RNA isolation. First strand cDNA was generated using iScript (bio-rad). Gene expression levels in CLL, Mec1 and B cells were determined using taqman assays (ThermoFisher) for Lig1 (Hs01553527_m1), XRCC1 (Hs00959834_m1), PARP1 (Hs00242302_m1) with 18S rRNA as controls (Hs99999901_s1).

Nuclease induced chromosomal deletions

Cas9 constructs specific for chr17 position 41,621,709 (KRT17 locus) were generated by cloning annealed oligos (RG1087 5'-ccggGGTGGGTGGTGAGATCAATG-3' and RG1088 5'-aaacCATTGATCTCACCACCCACC-3') into prelinearized pGuide-it-ZsGreen1 Vector (Clontech). TALENs specific for chr17 position 40,819,524-40,819,583 (KRT10 locus) were kindly provided by Oliver March (Paracelsus Private Medical University Salzburg, Austria). The CLL cell line Mec1 (21) was incubated for 6h in RPMI medium supplemented with or without 30µM Lig1/3 inhibitor L67 followed by Amaxa nucleofection (Lonza) with TALEN/Cas9 constructs. Cells were kept on RPMI medium supplemented with or without L67 for further 2 days prior sorting of GFP positive cells on a FACS AriaIII (Beckton Dickinson; purity ≥94.1% GFP+) and isolation of DNA (Qiagen). Chromosomal deletions were PCR amplified using Phusion polymerase and specific primers (RG1142 5'-TGGCATCTTCTTGGGGTTTA-3' and RG1143 5'-CCACATCCCCTTTTTCCATA-3'). For amplicon sequencing, PCR products from 50ng template DNA from two independent experiments were pooled and sent for sequencing on the miseq platform (Illumina). For quantification of chromosomal deletions, input DNA from cells descending from four independent experiments was titrated from 25ng to 1.56ng and subjected to PCR using primers RG1142/RG1143 and HotStar Taq DNA polymerase (Qiagen).

Cells and cell lines

293 cells, Mec1 cells and primary cells were cultured in RPMI Medium supplemented with 10% fetal calf serum (Gibco). Mec1 cells were authenticated by DNA fingerprinting and cytometrical analysis of surface markers (DSMZ). After purchase, stocks of Mec1 cells were frozen and passaged less than 6 months. 293 cells were provided by Stefan Hainzl (EB House

Austria, Salzburg) and periodically authenticated by morphologic inspection. Mec1 and 293 cells were confirmed by fingerprinting at the DMSZ (Braunschweig, Germany) on October 9th 2017. Mec1 and 293 cells were tested negative for mycoplasma in September 2017 using PCR based mycoplasma detection from cell culture supernatants (PanReac AppliChem). Primary cells were isolated from peripheral blood of CLL patients upon informed consent according to the national guidelines and of the ethics committee and according to the declaration of Helsinki (Ethics committee approval Salzburg: 415-E/1287/4–2011, 415-E/1287/8–2011). CLL cells and B cells were purified untouched using EasySep system (StemCell Technologies) or MACS (Miltenyi Biotec). Patient characteristics are summarized in supplementary table S1. The determination of prognostic markers and FISH analysis for trisomy 12, del11q, del13q, del17p was performed routinely at our department as previously described(22). In addition, FISH and karyogram analysis of sample 9956 (patient ID660) was performed at the laboratory for molecular biology and tumor cytogenetics at the Ordensklinikum Linz, Seilerstätte 4, 4010 Linz, Austria.

For cell cycle analysis, purified B and CLL cells were stained using CD5-FITC (clone: UCHT2; eBioscience) and CD19-PE/Cy7 (clone: SJ25C1; eBioscience) antibodies in PBS at room temperature. Cells were resuspended in prewarmed RPMI without Phenol-Red and stained with vybrant cell cycle dye (Vybrant® DyeCycle™ Violet Stain, V35003; ThermoFisher) for 1h at 37°C followed by immediate analysis by flow cytometry (Gallios, Beckman Coulter)

Sequence analysis and Bioinformatics.

Paired end fastq files were acquired by eurofins genomics and GATC-Biotech (Germany). Raw reads were trimmed and selected for paired reads using Trimmomatic v0.33(23)(PE mode, -phred 33,TRAILING:4), resulting in 8,378,777 paired reads surviving (95.56 % of input

reads). Forward and reverse reads were merged using FLASh v1.2.11(24) (-r 300 –f 350 –s 35) and 6,932,326 stiched sequences remained for further analysis. Only merged reads flanked by forward and reverse primers were regarded for further data analyses (only <0.001% of the resulting sequences were forward-forward or reverse-reverse primed; supplementary table S5). To avoid missing imprecise repair junctions of resected substrates, we decided to use the unique 6 bp stretch 3' of the conserved primer binding sites for mapping. Analyses of read length, frequency and sequence were performed using custom BASH and PERL scripts, which can be provided upon request. Sequence alignment for detection of deletions was perfomed using MAFFT alignment program(25). Circos plots were created in R using the *circlize* package (v0.3.8). All other graphs were created in Graph Pad Prism 5 and Inkscape v0.91.

Results

Next generation sequencing-assay for detecting repair of different DNA end structures

To test the efficiency of DSB repair, we set up a plasmid based repair assay, consisting of a pool of nine plasmids which harbor individual 350bp inserts flanked by conserved primer binding sites (Fig 1A, supplementary Fig S1). Upon digestion with respective restriction enzymes, the individual plasmids yield defined DNA break structures ranging from blunt ends with and without a 6bp microhomology to cohesive and non-cohesive 3' and 5' protruding ends with 4 nt overhangs (Fig 1B). Upon transfection into primary cells, the linear DNA substrates are recognized by the DNA DSB repair machinery and rejoined. The resulting repair junctions can subsequently be PCR-amplified using the conserved primer binding sites and analysed by next generation sequencing (NGS). As each of the nine plasmids harbors a unique DNA sequence between the conserved primer binding sites, all reads obtained by

NGS can be exactly mapped to the respective plasmids, allowing examination of efficiency and accuracy of DNA repair in context of DNA end structures and microhomologies.

DSB repair favors incompatible DNA ends in CLL cells

To detect aberrant DSB repair in CLL cells, we used our pool of linearized plasmid substrates to nucleofect primary CLL cells (CLL-Mut n=4, CLL-UM n=3; patient details shown in supplementary table S1) and B cells from healthy controls (n=3). Three days after nucleofection, we isolated DNA and PCR amplified repair junctions from each sample. Notably, we observed repaired substrates immediately after nucleofection in some CLL samples, which is in line with published data on rapid end joining of DNA ends (Fig 1C)(26). Upon NGS of pooled amplicons, we obtained a total of 2.676,354 reads, ranging from 96,000 to 587,418 reads for all samples (Fig 1D).

By calculating the ratio of inter- to intramolecular repair events, we surprisingly obtained a robust bias towards intermolecular repair junctions in CLL samples, irrespective of the BCR mutation status (CLL-Mut and CLL-UM), whereas normal B cells preferred an intramolecular repair (ratio inter/intramolecular repair CLL mean 1.88±0.71 STD; B cells 0.79±0.22, p=0.017 Mann Whitney test; Fig 2A). In particular, we observed significantly increased intermolecular repair of incompatible DNA ends in CLL cells compared to B cells (eg joining of plasmid #6 with plasmid #2 or plasmid #8 with plasmid #5) whereas compatible 3’ and 5’ overhangs or blunt ends were repaired at comparable efficiency (Fig 2B; supplementary table S2). None of the repair junctions were significantly overrepresented in B cells compared to CLL cells (Fig 2B; supplementary table S2). Also by analyzing only intramolecular repair frequencies of the nine different DNA break structures, we observed that non-cohesive 5’ ends (substrate #5) as well as incompatible 3’-5’ overhangs (substrate

#7) were repaired with significantly higher efficiency in CLL cells compared to B cells (substrate #5: CLL mean percentage of reads 4.8±2.4 STD, B cells 0.7±0.5; p=0.004; substrate #7: CLL mean 12.4±5.6 STD, B cells 2.5±2.4; p=0.005 two-tailed t-test assuming unequal variances; Fig 2C and supplementary table S3).

More end resection occurs during DSB repair in CLL cells

We next aimed at determining differences in the occurrence of deletions at repair junctions between CLL and B cells, resulting from joining of end resected DNA ends. Therefore, we first identified the most frequent repair junction for CLL-Mut, CLL-UM, and B cells for all individual intramolecular repair events and mapped all shorter sequences to the most frequent consensus. We thereby found that the most frequent repair junctions of the nine DNA substrates were the same within each sample group (CLL-Mut, CLL-UM, B cells; Fig 3A): blunt ends - irrespective of a 6bp microhomology – and cohesive 3' and 5' ends were preferably simply rejoined, whereas 1bp microhomologies were preferentially used when repairing non-cohesive 3' (substrate #3, Fig 3A) and 5' overhangs (substrate #5, Fig 3A). Incompatible 3'-5' overhangs (substrate #7), 3' overhang/blunt and 5' overhang/blunt ends (substrate #8 and #9) were preferentially joined and the ssDNA gaps filled up (Fig 3A).
We next graphically illustrated the occurrence of deletions at repair joints which we discerned by NGS. In all cases, deletions clustered around the repair junction of the most frequent consensus sequences (Fig 3B). By comparing the median numbers of resected bases (deletions) at repair junctions, we found that deletions were significantly more frequent in CLL cells compared to B cells (differences in the median number of deleted bases per sequence were significant with $p<0.0001$ between CLL-Mut and B cells and CLL-

UM and B cells for each substrate; except substrate #4 CLL-UM versus B cells: p=0.13; Wilcoxon rank sum test with continuity correction; Fig 3C).

DNA DSB repair is skewed towards MMEJ in CLL

Upon analyzing the sequences harboring deletions at the repair junction, we observed a high incidence of 1-9bp microhomologies flanking the deleted region irrespective of the sample group (CLL and B cells; supplementary Fig S2). As these microhomologies could at least in part derive from repair by MMEJ and as deletions were occurring at higher incidence in CLL (Fig 3), this prompted us to test whether the MMEJ pathway is generally more active in CLL compared to B cells. To this end, we more thoroughly analysed repair junctions of substrate #2, featuring a 6bp microhomology at both DNA ends. As already shown by Verkaik and coworkers using a similar approach, repair by the MMEJ pathway leads to deletion of one of the two 6bp microhomologies, whereas repair by c-NHEJ results in direct joining of the DNA ends, yielding a direct repeat of 6bp within the repair junction(27). Hence, calculating the ratio of the number of junctions deriving from 6bp microhomology mediated versus direct joining of substrate #2 reflects MMEJ versus c-NHEJ activity. As shown in Fig 4A, we found that direct joining of substrate #2 was the preferred repair mechanism in CLL as well as in B cells, however, repair by MMEJ was significantly increased relative to c-NHEJ in CLL cells, irrespective of BCR mutation status (ratio microhomology-mediated/direct joining of substrate #2 for CLL: mean 0.067±0.023 STD, B cells 0.024±0.005 STD; p=0.017 Mann Whitney test; Fig 4A).

Efficient joining of incompatible DNA ends in CLL is not exclusively dependent on microhomologies

Next, we tested whether CLL-specific efficient joining of incompatible DNA ends was solely dependent on MH-based repair of end-resected substrates. To test this, we only considered repair junctions mapping to the most frequently occurring sequence of a particular repaired substrate and calculated their relative frequencies, without considering repair of resected substrates. Thereby we found that again various incompatible DNA ends were more efficiently repaired in CLL cells compared to B cells, leading to a total of 12 junctions which were significantly overrepresented in CLL samples (Fig 4B and supplementary table S4). Again, none of the repair events were significantly overrepresented in B cells compared to CLL cells (Fig 4B and supplementary table S4). Though 7 out of these 12 junctions revealed short microhomologies (1 to 5 nt, supplementary table S4), 5 of these junctions were generated by direct intermolecular joining of 3'-5' overhangs or 5' overhang-blunt ends, implying that incompatible DNA ends were more efficiently joined in CLL cells also independent from terminal microhomologies (Fig 4C, supplementary table S4).

To elucidate the underlying mechanism for biased DSB DNA repair in CLL cells, we first analysed cell cycle stages in CLL and B cells (supplementary Fig S3). However, both CLL samples as well as B cells were mostly in G1 phase (range 90.2-95.2% for CLL; 87.5-97.5% for B cells) with no apparent cell cycle differences (supplementary Fig S3). We next examined expression levels of key factors involved in MMEJ and c-NHEJ in CLL and B cells (9). By extracting data from Haslinger and coworkers(28) using the oncomine database(29) (www.oncomine.org), we found that several genes, including PARP1, XRCC1 (forming a complex with Lig3) and Lig1, which all are involved in MMEJ were significantly upregulated in CLL compared to normal B cells (Fig 5A). In contrast, within the set of factors involved in c-NHEJ, only DNA-PKcs (PRKDC) and PARP3 showed a slight but significant overexpression in CLL and none of the factors examined showed downregulation in CLL (Fig 5A). To validate

expression of MMEJ factors in our CLL samples, we performed realtime RT-PCRs. Consistently, Lig1, XRCC1 and PARP1 were all higher expressed in CLL samples compared to B cells from healthy donors (supplementary Fig S4). As increased expression levels of MMEJ-specific factors could likely be causative for our observed bias towards MMEJ in CLL cells, we finally wanted to test whether PARP1, Lig1 or Lig3/XRCC1 could also contribute to MH-independent joining of incompatible ends, in particular intermolecular joining of 5' overhangs with blunt ends which we particularily observed to be increased in CLL samples (Fig 4B, C). Therefore, we performed a 293 based assay for direct joining of two GFP-based reporter constructs (pGFP-1 and pGFP-2) which encode a functional GFP protein only upon intermolecular direct joining of pGFP-1 (encoding the N-terminal portion of GFP with a 4 nt 5' overhang) and pGFP-2 (encoding the C-terminal portion of GFP starting with a blunt end) (Fig 5B). GFP expression based on direct joining of pGFP-1/pGFP-2 was analysed in presence of specific inhibitors targeting PARP (Olaparib), Lig1/3 (L67), and DNA-PKc (NU7441) as control. To normalize for transfection efficiencies, we cotransfected a plasmid encoding mCherry (pmCherry). As expected, direct repair of the GFP plasmids was strongly impeded by inhibition of DNA-PKcs, which are central to c-NHEJ. To a lesser extent also inhibition of Lig1/3 showed an effect on direct pGFP-1/pGFP-2 joining, while inhibition of PARP family proteins by Olaparib had no effect on DNA repair in this assay (Fig 5C).

Induction of chromosomal deletions in the CLL cell line Mec1 is impaired upon inhibition of Lig1/3

Finally, we tested whether Lig1 or XRCC1/Lig3 is involved in the generation of chromosomal deletions between a 5'overhang DNA DSB and a blunt end DNA DSB in CLL. Therefore, we transiently transfected the CLL cell line Mec1 with constructs expressing TALENs (generating

a 5'overhang) and Cas9 (generating blunt end DSBs), which both cleave at chromosome 17, with or without treatment with 30µM Lig1/3 inhibitor L67 (Fig 6A). Of note, realtime RT-PCR revealed that in Mec1 cells, MMEJ specific factors Lig1, XRCC1 and PARP1 were also more abundantly expressed than in normal B cells (supplementary Fig S4). We positively sorted transfected cells based on GFP expression from the Cas9 construct and estimated chromosomal deletion frequencies of a large 0.8Mb fragment by PCR on serially diluted input DNA isolated from sorted cells (Fig 6A, B). As estimated from four independent experiments, the chromosomal deletion frequency of L67 treated cells was lower compared to untreated cells, as amplification of breakpoint junctions failed from 1.56ng input DNA of L67 treated cells in all experiments, whereas in two of four experiments, PCR amplified breakpoint junctions were detectable in untreated cells at that DNA concentration (Fig 6B). Amplicon sequencing of the PCR products from two experiments revealed that L67 treated Mec1 cells had an increased frequency of short (5-49bp) deletions at the breakpoint junction, whereas large (≥50bp) deletions were reduced (Fig 6C), again pointing to involvement of Lig1/3 in the occurrence of large deletions at repair joints. Small (0-4bp) deletions, likely resulting from direct joining or deletions within the 5' overhang were also reduced in L67 treated cells (Fig 6C).

Thus, we infer that the described overexpression of Lig1 or XRCC1 in CLL could explain the observed bias towards both, MMEJ as well as increased repair of incompatible DNA ends with increased deletions at repair junctions.

Discussion

Aberrant repair of DSB can lead to genetic changes, driving carcinogenesis and clonal evolution of cancer. Here we describe several differences of DSB repair in B cells versus CLL

cells by applying a plasmid based repair assay analyzed by NGS as well as by assessing repair of TALEN/Cas9 induced chromosomal deletions in the Mec1 cell line. While plasmid based assays have been used in the past to investigate DSB repair in cell lines and cancer cells(27;30;31), our NGS based approach allowed simultaneous analysis of efficiency and accuracy of DSB repair in regard to diverse DNA break structures and the cellular context at single nucleotide level. In general, our assay revealed that complementary 5' protruding ends as well as blunt ends exhibited highest repair efficiency and 3' cohesive and 3' non-cohesive staggered ends showing weakest joining efficiency. Weak repair of 3' overhangs was noted in earlier studies(31), probably because 3' overhangs rather promote homologous recombination (HR) as they are required for strand exchange reaction in HR(32;33). However, our repair assay revealed a complex set of substantial differences in efficiency as well as precision of DNA repair in CLL vs B cells. In addition to the frequent occurrence of deletions at the repair junction, which was already described for leukemic cells(30), our assay revealed that non-cohesive protruding ends were joined significantly more efficiently in CLL cells compared to B cells.

In our study, efficient joining of incompatible ends was attributed to increased MMEJ activity, reflected by the presence of short microhomologies within repair junctions of end resected incompatible DNA substrates. Concurrently, a 6bp microhomology was preferentially used in CLL cells for repair of DNA substrates. These results indicate that DNA DSB repair is skewed towards MMEJ in CLL, which is corroborated by overexpression of MMEJ specific factors in CLL. Notably, this skewing towards MMEJ does not result from cell cycle differences, as nucleofected CLL cells in our analysis were also G1 arrested. We further observed CLL-specific increased joining of incompatible DNA ends independent from end resection and usage of microhomologies. Strikingly, this increased joining efficiency was

especially pronounced in intermolecular repair events, indicating a somehow increased promiscuity in DNA end joining. While MMEJ classically involves end resection of DNA overhangs after stabilization of the paired homologous region by several nucleases(34;35), direct joining of incompatible protruding ends can be mediated by two possibilities: either DNA ends are blunted prior to DNA joining (refilled or resected) or otherwise DNA is re-synthesised across a stabilized DNA junction of two staggered DNA ends by polymerase μ or λ, followed by ligation of DNA nicks(36-38). While ligation of blunted dsDNA ends is normally mediated by Lig4/XRCC4, nick sealing is efficiently performed by Lig1 and Lig3/XRCC1 complexes (39;40). Our pGFP-1/pGFP-2 repair assay revealed that while most repair events are catalyzed by c-NHEJ involving DNA-PKcs, repair could partly be mediated by polymerase-dependent DNA synthesis across direct pGFP-1/pGFP-2 junctions followed by nick-sealing by Lig1/3. In that way, overexpression of Lig1/3 could not only contribute to increased MMEJ but also to direct joining of incompatible DNA ends. Lig4 deficient cell lines are still able to repair DNA DSBs, albeit the number of direct joints are decreased and MH usage is increased due to activity of Lig1/3 (41;42). While sole activity of Lig1/3 in Lig4 deficient cells led to a higher frequency of endonuclease induced translocations in rodent cell lines, the frequency in human cell lines was decreased, showing that efficiency and kinetics of DNA DSB repair is likely depending on cell type and species specific expression levels of repair factors (41;43). Our own data suggest that Lig1/3 may significantly contribute to the formation of TALEN/Cas9 induced large chromosomal deletions in the CLL cell line Mec1 as we observed a reduction in their occurrence upon Lig1/3 inhibition, together with a reduction in large deletions at repair joints. Hence, our results would propose that CLL specific increased expression levels of the MMEJ factors Lig1 and XRCC1 could contribute to increased propensity to acquire chromosomal aberrations during DNA

DSB repair. This fits with the observation that chromosomal aberrations are frequently found to be subclonal in CLL, pointing to their successive generation during disease progression (6). In addition, an increased MMEJ activity could also explain the formation of small deletions and microdeletions frequently observed in CLL(44) and also in other cancer entities (45). These deletions often exhibit sequence homologies at breakpoint junctions, suggesting that they likely arise due to MMEJ of DNA DSBs. Alternatively, they could occur by polymerase slippage during replication (46;47). As we observed several differences in end joining between CLL and B cells, it would be certainly interesting to screen DNA repair quality/quantity in therapy sensitive versus refractory samples as well as in other clinically relevant CLL subsets (such as samples with complex karyotype). Deriano and coworkers already reported increased error-prone end joining of DNA ends in CLL cells obtained from a therapy resistant patient (48). Hence, it is conceivable that CLL subset or risk group specific differences in DNA DSB repair could contribute to diverse clinical outcomes.

Although a portion of CLL patients exhibits mutations at DNA repair genes (6), our data rather suggest an inherently aberrant DNA DSB repair activity in CLL due to different expression levels of key factors for MMEJ, in particular as we excluded del(11q) and del(17p) patients (harboring deleted *ATM* and *p53* genes) and as all samples included in our analyses showed a very uniform pattern of repair junction formation, irrespective of the BCR mutation status.

Summarizing, we could identify profound differences in efficiency and precision of DSB repair between CLL cells and normal B cells. Considering a reported increased formation of DNA DSBs in precancerous lesions and cancers(49), their imprecise repair due to increased Lig1 and XRCC1 levels could thus continuously enhance the formation of genomic aberrations, contributing to clonal evolution and chemoresistance. Hence, concomitant

usage of Lig1/3 inhibitors during CLL treatment would not only potentiate cytotoxicity of DNA damaging agents (50) but might also impede clonal evolution by acquisition of novel genomic rearrangements.

Acknowledgements

We thank Oliver March (Salzburg) for providing TALENs and Markus Steiner (Salzburg) for cell sorting.

Reference List

(1) Alexandrov LB, Nik-Zainal S, Wedge DC, Aparicio SA, Behjati S, Biankin AV, et al. Signatures of mutational processes in human cancer. Nature 2013 Aug 22;500(7463):415-21.

(2) Stephens PJ, McBride DJ, Lin ML, Varela I, Pleasance ED, Simpson JT, et al. Complex landscapes of somatic rearrangement in human breast cancer genomes. Nature 2009 Dec 24;462(7276):1005-10.

(3) Stephens PJ, Greenman CD, Fu B, Yang F, Bignell GR, Mudie LJ, et al. Massive genomic rearrangement acquired in a single catastrophic event during cancer development. Cell 2011 Jan 7;144(1):27-40.

(4) Burger JA, Landau DA, Taylor-Weiner A, Bozic I, Zhang H, Sarosiek K, et al. Clonal evolution in patients with chronic lymphocytic leukaemia developing resistance to BTK inhibition. Nat Commun 2016;7:11589.

(5) Landau DA, Tausch E, Taylor-Weiner AN, Stewart C, Reiter JG, Bahlo J, et al. Mutations driving CLL and their evolution in progression and relapse. Nature 2015 Oct 22;526(7574):525-30.

(6) Landau DA, Carter SL, Stojanov P, McKenna A, Stevenson K, Lawrence MS, et al. Evolution and impact of subclonal mutations in chronic lymphocytic leukemia. Cell 2013 Feb 14;152(4):714-26.

(7) Lieber MR. The mechanism of double-strand DNA break repair by the nonhomologous DNA end-joining pathway. Annu Rev Biochem 2010;79:181-211.

(8) Lieber MR, Gu J, Lu H, Shimazaki N, Tsai AG. Nonhomologous DNA end joining (NHEJ) and chromosomal translocations in humans. Subcell Biochem 2010;50:279-96.

(9) Chiruvella KK, Liang Z, Wilson TE. Repair of double-strand breaks by end joining. Cold Spring Harb Perspect Biol 2013 May;5(5):a012757.

(10) Kent T, Chandramouly G, McDevitt SM, Ozdemir AY, Pomerantz RT. Mechanism of microhomology-mediated end-joining promoted by human DNA polymerase theta. Nat Struct Mol Biol 2015 Mar;22(3):230-7.

(11) Meyer D, Fu BX, Heyer WD. DNA polymerases delta and lambda cooperate in repairing double-strand breaks by microhomology-mediated end-joining in Saccharomyces cerevisiae. Proc Natl Acad Sci U S A 2015 Dec 15;112(50):E6907-E6916.

(12) Hamblin TJ, Davis Z, Gardiner A, Oscier DG, Stevenson FK. Unmutated Ig V(H) genes are associated with a more aggressive form of chronic lymphocytic leukemia. Blood 1999 Sep 15;94(6):1848-54.

(13) Hartmann TN, Pleyer L, Desch P, Egle A, Greil R. Novel therapeutics approaches to chronic lymphocytic leukemia based on recent biological insights. Discov Med 2009 Oct;8(42):157-64.

(14) Pleyer L, Egle A, Hartmann TN, Greil R. Molecular and cellular mechanisms of CLL: novel therapeutic approaches. Nat Rev Clin Oncol 2009 Jul;6(7):405-18.

(15) Rowley JD. Chromosomal translocations: revisited yet again. Blood 2008 Sep 15;112(6):2183-9.

(16) Dicker F, Schnittger S, Haferlach T, Kern W, Schoch C. Immunostimulatory oligonucleotide-induced metaphase cytogenetics detect chromosomal aberrations in 80% of CLL patients: A study of 132 CLL cases with correlation to FISH, IgVH status, and CD38 expression. Blood 2006 Nov 1;108(9):3152-60.

(17) Haferlach C, Dicker F, Schnittger S, Kern W, Haferlach T. Comprehensive genetic characterization of CLL: a study on 506 cases analysed with chromosome banding analysis, interphase FISH, IgV(H) status and immunophenotyping. Leukemia 2007 Dec;21(12):2442-51.

(18) Puente XS, Pinyol M, Quesada V, Conde L, Ordonez GR, Villamor N, et al. Whole-genome sequencing identifies recurrent mutations in chronic lymphocytic leukaemia. Nature 2011 Jul 7;475(7354):101-5.

(19) Puente XS, Bea S, Valdes-Mas R, Villamor N, Gutierrez-Abril J, Martin-Subero JI, et al. Non-coding recurrent mutations in chronic lymphocytic leukaemia. Nature 2015 Oct 22;526(7574):519-24.

(20) Kim H, Kim JS. A guide to genome engineering with programmable nucleases. Nat Rev Genet 2014 May;15(5):321-34.

(21) Stacchini A, Aragno M, Vallario A, Alfarano A, Circosta P, Gottardi D, et al. MEC1 and MEC2: two new cell lines derived from B-chronic lymphocytic leukaemia in prolymphocytoid transformation. Leuk Res 1999 Feb;23(2):127-36.

(22) Tinhofer I, Rubenzer G, Holler C, Hofstaetter E, Stoecher M, Egle A, et al. Expression levels of CD38 in T cells predict course of disease in male patients with B-chronic lymphocytic leukemia. Blood 2006 Nov 1;108(9):2950-6.

(23) Bolger AM, Lohse M, Usadel B. Trimmomatic: a flexible trimmer for Illumina sequence data. Bioinformatics 2014 Aug 1;30(15):2114-20.

(24) Magoc T, Salzberg SL. FLASH: fast length adjustment of short reads to improve genome assemblies. Bioinformatics 2011 Nov 1;27(21):2957-63.

(25) Katoh K, Standley DM. MAFFT multiple sequence alignment software version 7: improvements in performance and usability. Mol Biol Evol 2013 Apr;30(4):772-80.

(26) Mao Z, Bozzella M, Seluanov A, Gorbunova V. Comparison of nonhomologous end joining and homologous recombination in human cells. DNA Repair (Amst) 2008 Oct 1;7(10):1765-71.

(27) Verkaik NS, Esveldt-van Lange RE, van HD, Bruggenwirth HT, Hoeijmakers JH, Zdzienicka MZ, et al. Different types of V(D)J recombination and end-joining defects in DNA double-strand break repair mutant mammalian cells. Eur J Immunol 2002 Mar;32(3):701-9.

(28) Haslinger C, Schweifer N, Stilgenbauer S, Dohner H, Lichter P, Kraut N, et al. Microarray gene expression profiling of B-cell chronic lymphocytic leukemia subgroups defined by genomic aberrations and VH mutation status. J Clin Oncol 2004 Oct 1;22(19):3937-49.

(29) Rhodes DR, Yu J, Shanker K, Deshpande N, Varambally R, Ghosh D, et al. ONCOMINE: a cancer microarray database and integrated data-mining platform. Neoplasia 2004 Jan;6(1):1-6.

(30) Gaymes TJ, Mufti GJ, Rassool FV. Myeloid leukemias have increased activity of the nonhomologous end-joining pathway and concomitant DNA misrepair that is dependent on the Ku70/86 heterodimer. Cancer Res 2002 May 15;62(10):2791-7.

(31) Poplawski T, Pastwa E, Blasiak J. Non-homologous DNA end joining in normal and cancer cells and its dependence on break structures. Genet Mol Biol 2010 Apr;33(2):368-73.

(32) Broderick R, Nieminuszczy J, Baddock HT, Deshpande RA, Gileadi O, Paull TT, et al. EXD2 promotes homologous recombination by facilitating DNA end resection. Nat Cell Biol 2016 Mar;18(3):271-80.

(33) Liu T, Huang J. DNA End Resection: Facts and Mechanisms. Genomics Proteomics Bioinformatics 2016 Jun;14(3):126-30.

(34) Davis AJ, Chen DJ. DNA double strand break repair via non-homologous end-joining. Transl Cancer Res 2013 Jun;2(3):130-43.

(35) Truong LN, Li Y, Shi LZ, Hwang PY, He J, Wang H, et al. Microhomology-mediated End Joining and Homologous Recombination share the initial end resection step to repair DNA double-strand breaks in mammalian cells. Proc Natl Acad Sci U S A 2013 May 7;110(19):7720-5.

(36) Smith J, Baldeyron C, De O, I, Sala-Trepat M, Papadopoulo D. The influence of DNA double-strand break structure on end-joining in human cells. Nucleic Acids Res 2001 Dec 1;29(23):4783-92.

(37) Mahajan KN, Nick McElhinny SA, Mitchell BS, Ramsden DA. Association of DNA polymerase mu (pol mu) with Ku and ligase IV: role for pol mu in end-joining double-strand break repair. Mol Cell Biol 2002 Jul;22(14):5194-202.

(38) Pryor JM, Waters CA, Aza A, Asagoshi K, Strom C, Mieczkowski PA, et al. Essential role for polymerase specialization in cellular nonhomologous end joining. Proc Natl Acad Sci U S A 2015 Aug 18;112(33):E4537-E4545.

(39) Cannan WJ, Rashid I, Tomkinson AE, Wallace SS, Pederson DS. The Human Ligase IIIalpha-XRCC1 Protein Complex Performs DNA Nick Repair after Transient Unwrapping of Nucleosomal DNA. J Biol Chem 2017 Mar 31;292(13):5227-38.

(40) Chafin DR, Vitolo JM, Henricksen LA, Bambara RA, Hayes JJ. Human DNA ligase I efficiently seals nicks in nucleosomes. EMBO J 2000 Oct 16;19(20):5492-501.

(41) Ghezraoui H, Piganeau M, Renouf B, Renaud JB, Sallmyr A, Ruis B, et al. Chromosomal translocations in human cells are generated by canonical nonhomologous end-joining. Mol Cell 2014 Sep 18;55(6):829-42.

(42) Masani S, Han L, Meek K, Yu K. Redundant function of DNA ligase 1 and 3 in alternative end-joining during immunoglobulin class switch recombination. Proc Natl Acad Sci U S A 2016 Feb 2;113(5):1261-6.

(43) Lu G, Duan J, Shu S, Wang X, Gao L, Guo J, et al. Ligase I and ligase III mediate the DNA double-strand break ligation in alternative end-joining. Proc Natl Acad Sci U S A 2016 Feb 2;113(5):1256-60.

(44) Marinelli M, Peragine N, Di M, V, Chiaretti S, De Propris MS, Raponi S, et al. Identification of molecular and functional patterns of p53 alterations in chronic lymphocytic leukemia patients in different phases of the disease. Haematologica 2013 Mar;98(3):371-5.

(45) Rothenberg SM, Mohapatra G, Rivera MN, Winokur D, Greninger P, Nitta M, et al. A genome-wide screen for microdeletions reveals disruption of polarity complex genes in diverse human cancers. Cancer Res 2010 Mar 15;70(6):2158-64.

(46) Verdin H, D'haene B, Beysen D, Novikova Y, Menten B, Sante T, et al. Microhomology-mediated mechanisms underlie non-recurrent disease-causing microdeletions of the FOXL2 gene or its regulatory domain. PLoS Genet 2013;9(3):e1003358.

(47) Watson CT, Marques-Bonet T, Sharp AJ, Mefford HC. The genetics of microdeletion and microduplication syndromes: an update. Annu Rev Genomics Hum Genet 2014;15:215-44.

(48) Deriano L, Merle-Béral H, Guipaud O, Sabatier L, Delic J. Mutagenicity of non-homologous end joining DNA repair in a resistant subset of human chronic lymphocytic leukaemia B cells. Br J Haematol. 2006 Jun;133(5):520-5.

(49) Halazonetis TD, Gorgoulis VG, Bartek J. An oncogene-induced DNA damage model for cancer development. Science 2008 Mar 7;319(5868):1352-5.

(50) Tomkinson AE, Howes TR, Wiest NE. DNA ligases as therapeutic targets. Transl Cancer Res 2013 Jun;2(3).

Figure legends

Figure 1. Plasmid based DSB repair assay. (A) Schematic representation of plasmid based DSB repair. Circular plasmids are linearized upon digestion with restriction enzymes followed by transfection of cells where substrates are rejoined. Repair junctions are detected by PCR using conserved forward (fwd) and reverse (rev) primer binding sites on the plasmids. **(B)** DNA end structures of substrates used in our DSB repair assay (MH: microhomology of 6bp). **(C)** B cells and CLL cells were transfected with our pooled repair substrates #1-#9. DNA was isolated 72h (left panel) or 0h and 72h (right panel) post transfection and repair junctions were PCR amplified and run on an agarose gel. Amplicons corresponding to a 300bp band were gel excised and analysed by NGS. Asterisks refer to bands corresponding to amplified undigested plasmids. Amplicons from a control PCR on TP53 are loaded to show integrity of isolated DNA. **(D)** Number of reads obtained by NGS of the respective amplicons is shown.

Figure 2. DNA DSB repair in B cells and CLL cells. (A) Graph shows the ratio of inter- to intramolecular repair junctions. **(B)** Inter- and intramolecular repair events are depicted as circos plots for CLL cells and for normal B cells. The nine segments represent the nine different plasmids used in our repair assay. The size of the segments reflects their relative occurrence from NGS analysed repair junctions. Repair frequencies are indicated by size of ribbons, where orientation of repair of the respective substrates is given by arrowheads at the end of ribbons (mean values for CLL and B cells as shown in supplementary table S2 were used for generating plots; start of ribbon denotes forward primed arms; arrowhead of ribbon denotes reverse primed arm of substrates shown in supplementary Fig 1). Repair junctions significantly overrepresented in CLL cells compared to B cells (and vice versa) are colored red ($p<0.05$; two-tailed t-test with unequal variances) and light red ($0.05\leq p<0.1$), and the correspondingly underrepresented repair junctions are colored blue ($p<0.05$; two-tailed t-test with unequal variances) and light blue ($0.05\leq p<0.1$), respectively. **(C)** The frequency of intramolecular repair junctions for individual substrates is shown. Asterisks indicate significant differences between CLL and B cells (substrate #5: $p=0.004$; substrate #7: $p=0.005$ two-tailed t-test with unequal variances).

Figure 3. Deletions at repair junctions. (A) The most frequent repair junction for individual substrates is indicated. 1bp microhomologies used for repair are indicated in red. **(B)** Graphs show the occurrence of deletions at repaired substrates as horizontal lines. Y-axis gives the frequency of deletions and x-axis indicates the position of the deletion within the amplicon. **(C)** All sequences obtained for the respective sample cohort were analyzed based on deleted sequence lengths. Box plots show the median length of deletions within the 25^{th} and 75^{th} percentile (box) and data within a 1.5 times interquartile distance from the median as whiskers. Outliers (all other data points) are indicated as circles.

Figure 4. Microhomologies at repair junctions. (A) Ratio of repair junctions deriving from microhomology mediated joining (6bp microhomology, MH) versus direct joining of substrate #2 from transfected CLL and B cell samples. Asterisks indicates significant difference between CLL and B cells (p=0.017 Mann-Whitney test). **(B)** The most frequently used sequence for each of all individual inter- and intramolecular repair events are depicted as circos plots for CLL cells and for normal B cells. Circos plots were generated as indicated for Fig 2 (sequences shown in supplementary table S4). **(C)** Repair junctions which were significantly overrepresented in CLL ($p<0.05$ from B) are schematically depicted. The hash mark specifies the respective forward-primed (red) and reverse-primed (yellow) DNA substrate. Arrows indicate gap filling by DNA polymerases.

Figure 5. DNA DSB repair of non-resected DNA substrates. (A) Expression values for factors involved in MMEJ (left panel) and c-NHEJ (right panel) are shown as fold change between CLL and B lymphocytes. >2-fold differences are shaded grey. Significances are indicated above each bar. (CLL n=100; B cells n=11). **(B)** schematic representation of plasmids (GFP-1 and GFP-2) used to detect intermolecular repair of blunt/5'overhang junctions. Direct intermolecular repair of non-resected plasmids leads to GFP expression. **(C)** 293 cells were transfected using plasmids GFP-1 and GFP-2 shown in (B) together with a plasmid expressing mCherry. Representative FACS plots show GFP/mCherry expression in presence of inhibitors. Data within plots gives percentage of GFP^+-cells within all $mCherry^+$-cells. Graph shows the results from three independent FACS experiments. UTR1: untreated cells transfected using GeneJuice (controls for NU7441, Olaparib treated cells). UTR2: untreated cells transfected using nucleofection (controls for L67 treated cells). neg: cells transfected with mCherry plasmids only. Significant differences in comparison to untreated controls is indicated above the respective dataset (two-tailed t-test with unequal variances).

Figure 6. Induction of chromosomal deletions by TALEN/Cas9 generated DNA DSBs are dependent on Lig1/3. (A) Schematic representation of chromosomal deletions induced by TALENs/Cas9 constructs. Binding sites of TALENs and Cas9 constructs are shaded red and green, respectively. Genomic position and sequence of binding sites are shown in 5'-3' orientation. The protospacer adjacent motif is colored blue. Specific primers for amplification of breakpoint junctions are given as black arrows on chromosome 17, yielding an approximate 180bp PCR product in case a 0.8Mb fragment of chr17 is deleted. **(B)** Limiting dilution of genomic DNA to estimate the frequency of chromosomal deletions after expression of TALEN/Cas9 constructs in Mec1 cells treated with 30µM Lig1/3 inhibior L67 or untreated controls. PCR amplification was performed with serial dilutions of genomic DNA from four independent experiments as template (25, 12.5, 6.25, 3.125, and 1.56ng). A agarose gel from one experiment is shown. The number of times a PCR fragment was detected from four independent experiments is indicated below the gel. n.t.=Mec1 cells not transfected with TALEN/Cas9 constructs. **(C)** PCR products from two experiments were amplicon sequenced and fragment lengths were analysed (Mec1: 1,191,602 reads; Mec1

L67 treated: 177,319 reads). The percentage of reads with the respective amount of end resection are depicted in separate graphs, demonstrating the occurrence of about 8 times more fragments with large deletions (≥50bp) at breakpoint junctions. Percentages are indicated above the bars. (Reads with insertions at breakpoints are not depicted).

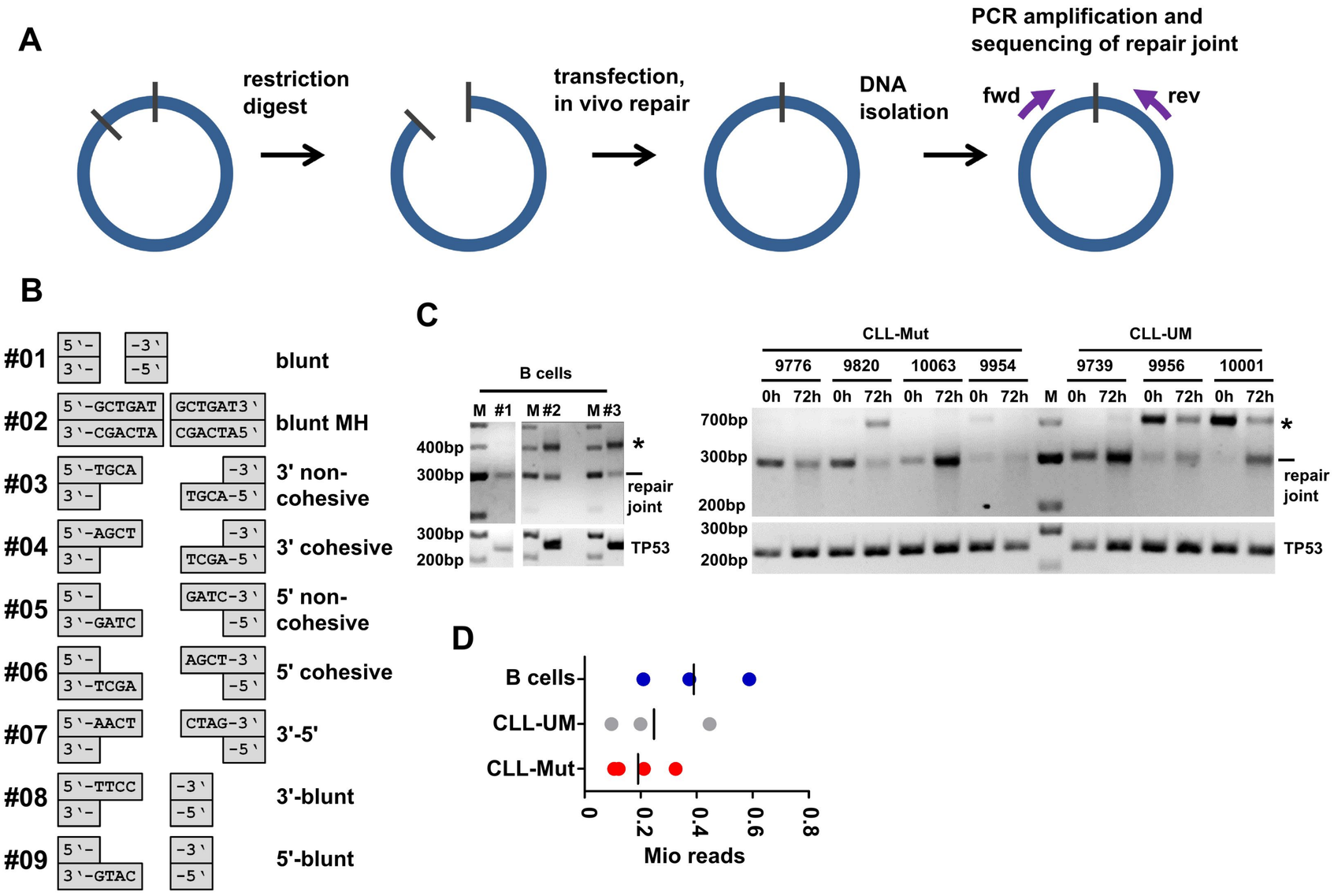
A
restriction digest
transfection, in vivo repair
DNA isolation
PCR amplification and sequencing of repair joint
fwd
rev
B
#01
#02
5'-GCTGAT
3'-CGACTA
GCTGAT3'
CGACTA5'
blunt MH
#03
5'-TGCA
3'-
-3'
TGCA-5'
3' non-cohesive
#04
5'-AGCT
3'-
-3'
TCGA-5'
3' cohesive
#05
5'-
3'-GATC
GATC-3'
-5'
5' non-cohesive
#06
5'-
3'-TCGA
AGCT-3'
-5'
5' cohesive
#07
5'-AACT
3'-
CTAG-3'
-5'
3'-5'
#08
5'-TTCC
3'-
-3'
-5'
3'-blunt
#09
5'-
3'-GTAC
-3'
-5'
5'-blunt
C
B cells
M #1
M #2
M #3
400bp
300bp
300bp
200bp
*
repair joint
TP53
CLL-Mut
9776
9820
10063
9954
CLL-UM
9739
9956
10001
0h 72h 0h 72h 0h 72h 0h 72h M 0h 72h 0h 72h 0h 72h
700bp
300bp
200bp
300bp
200bp
*
repair joint
TP53
D
B cells
CLL-UM
CLL-Mut
0
0.2
0.4
0.6
0.8
Mio reads

Figure 1

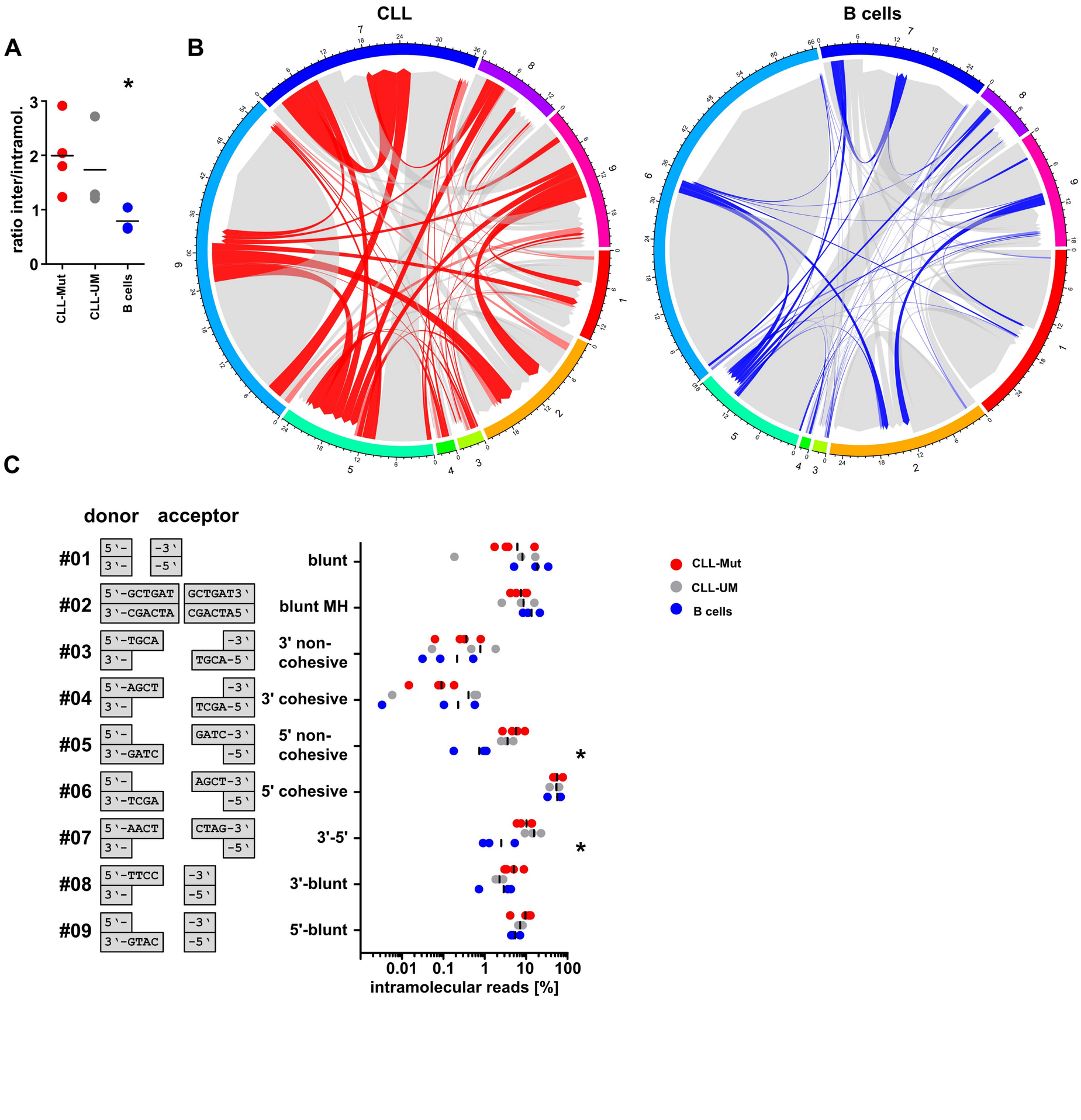
A
ratio inter/intramol.
3
2
1
0
*
CLL-Mut
CLL-UM
B cells
B
CLL
B cells
C
donor
acceptor
#01
5'-
3'-
-3'
-5'
blunt
#02
5'-GCTGAT
3'-CGACTA
GCTGAT3'
CGACTA5'
blunt MH
#03
5'-TGCA
3'-
-3'
TGCA-5'
3' non-cohesive
#04
5'-AGCT
3'-
-3'
TCGA-5'
3' cohesive
#05
5'-
3'-GATC
GATC-3'
-5'
5' non-cohesive
*
#06
5'-
3'-TCGA
AGCT-3'
-5'
5' cohesive
#07
5'-AACT
3'-
CTAG-3'
-5'
3'-5'
*
#08
5'-TTCC
3'-
-3'
-5'
3'-blunt
#09
5'-
3'-GTAC
-3'
-5'
5'-blunt
0.01
0.1
1
10
100
intramolecular reads [%]
CLL-Mut
CLL-UM
B cells

Figure 2

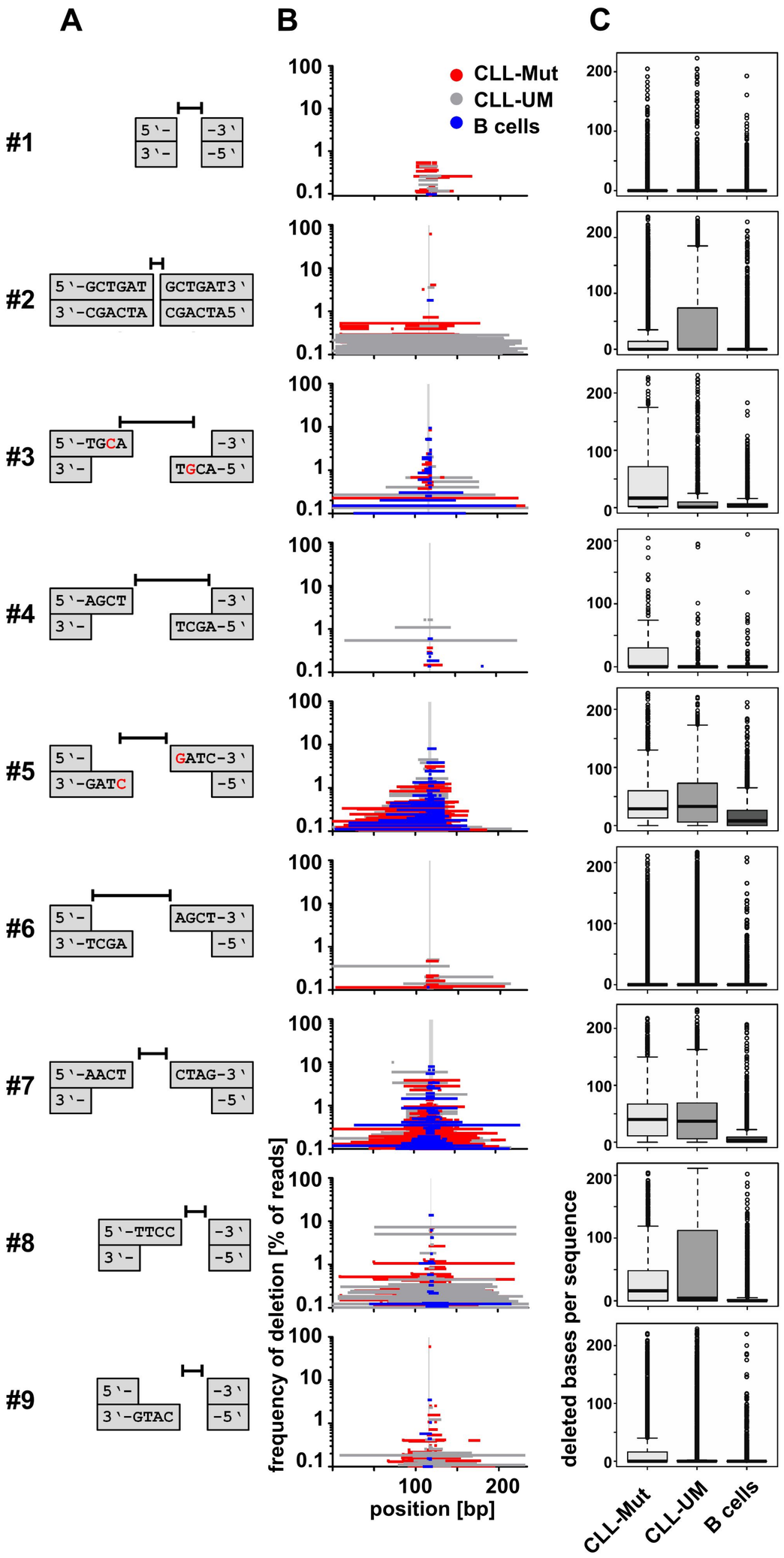
A
B
C
#1
5'-
-3'
3'-
-5'
#2
5'-GCTGAT
GCTGAT3'
3'-CGACTA
CGACTA5'
#3
5'-TGCA
-3'
3'-
TGCA-5'
#4
5'-AGCT
-3'
3'-
TCGA-5'
#5
5'-
GATC-3'
3'-GATC
-5'
#6
5'-
AGCT-3'
3'-TCGA
-5'
#7
5'-AACT
CTAG-3'
3'-
-5'
#8
5'-TTCC
-3'
3'-
-5'
#9
5'-
-3'
3'-GTAC
-5'
CLL-Mut
CLL-UM
B cells
frequency of deletion [% of reads]
position [bp]
deleted bases per sequence
CLL-Mut
CLL-UM
B cells

Figure 3

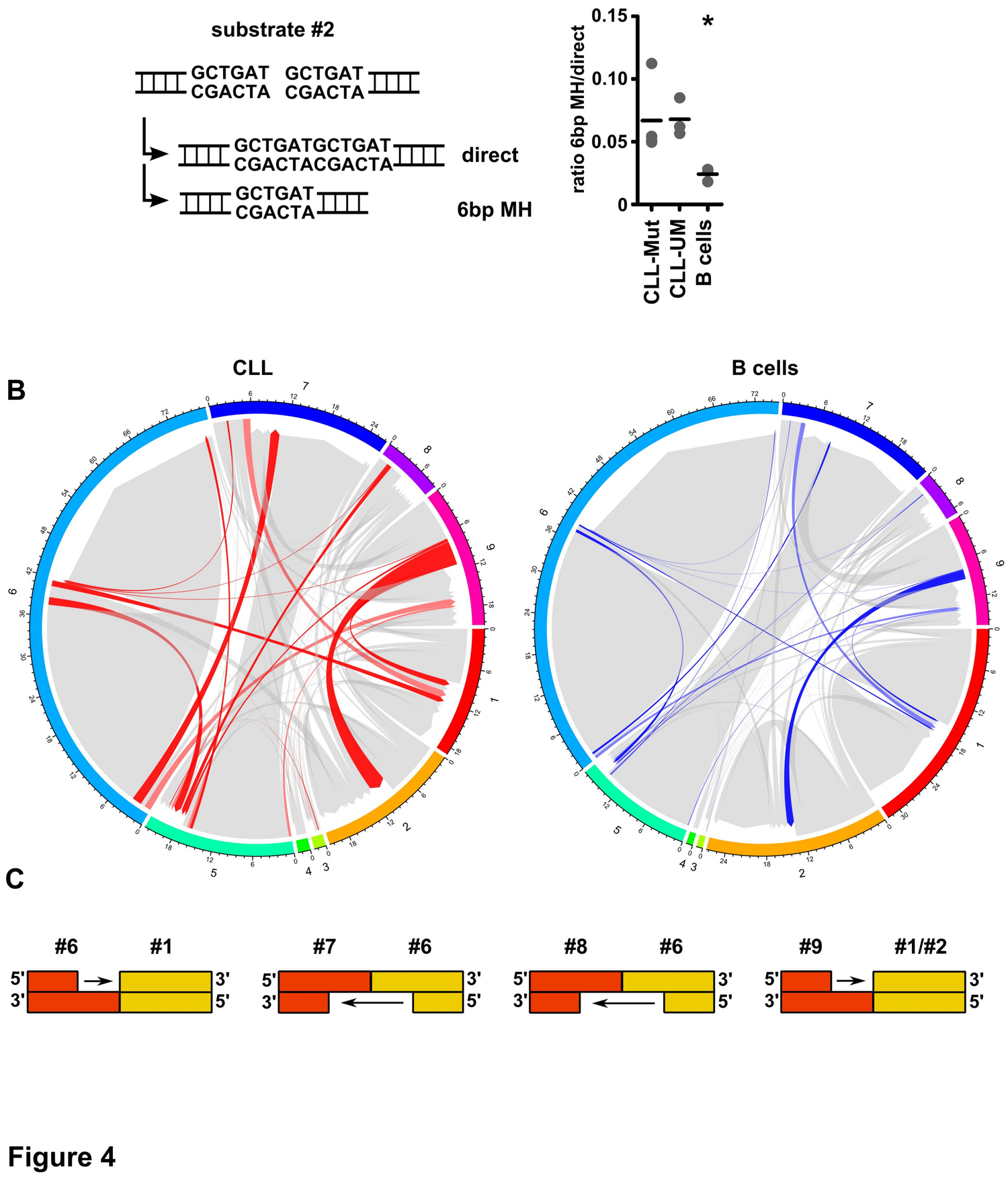
A
substrate #2
GCTGAT GCTGAT
CGACTA CGACTA
GCTGATGCTGAT
CGACTACGACTA
direct
GCTGAT
CGACTA
6bp MH
ratio 6bp MH/direct
0.15
0.10
0.05
0
*
CLL-Mut
CLL-UM
B cells
CLL
B cells
B
C
#6
#1
#7
#6
#8
#6
#9
#1/#2
5'
3'
3'
5'

Figure 4

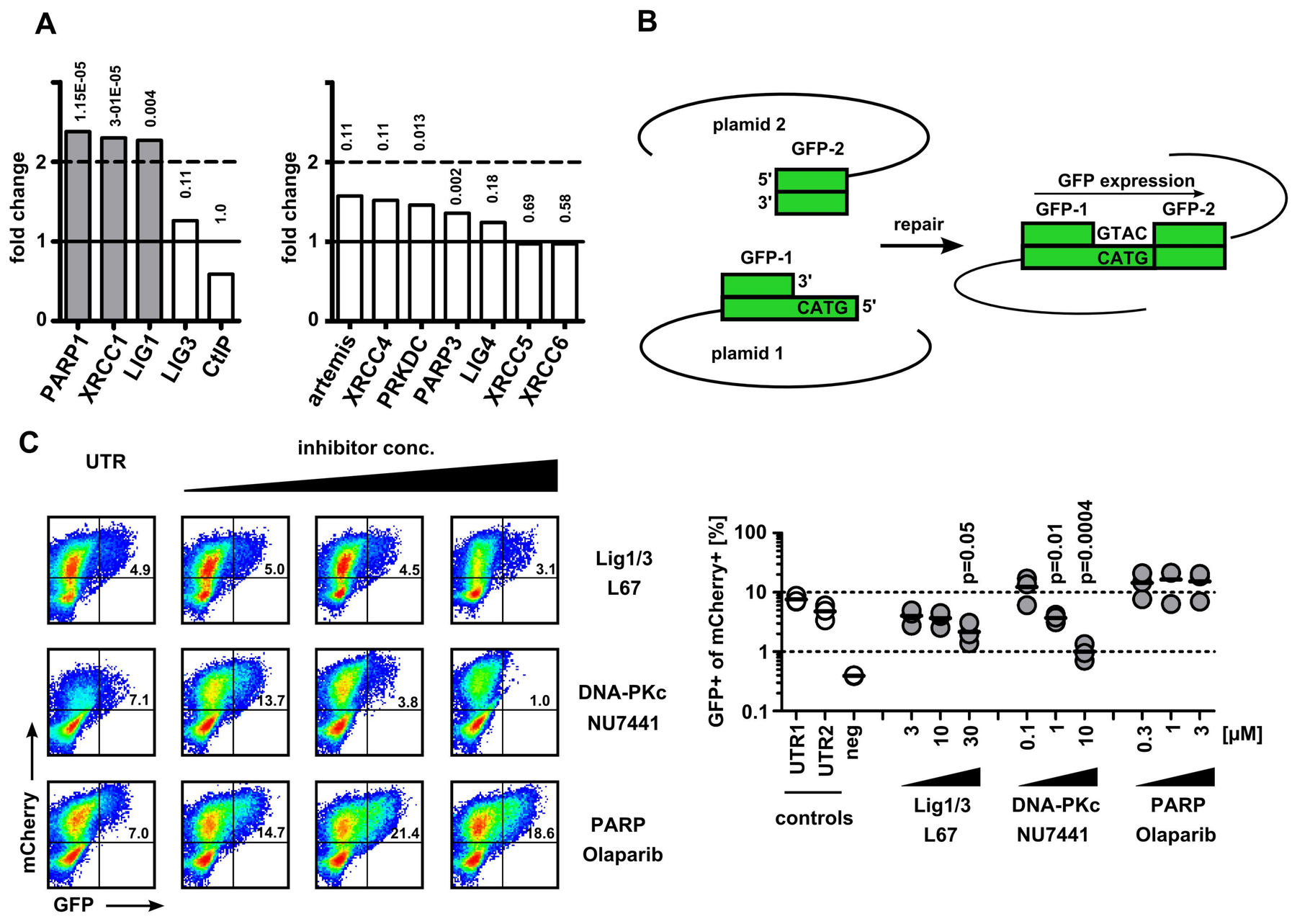
A
fold change
2
1
0
1.15E-05
3-01E-05
0.004
0.11
1.0
PARP1
XRCC1
LIG1
LIG3
CtIP
0.11
0.11
0.013
0.002
0.18
0.69
0.58
artemis
XRCC4
PRKDC
PARP3
LIG4
XRCC5
XRCC6
B
plamid 2
GFP-2
5'
3'
repair
GFP-1
3'
CATG
5'
plamid 1
GFP expression
GFP-1
GFP-2
GTAC
CATG
C
UTR
inhibitor conc.
4.9
5.0
4.5
3.1
Lig1/3
L67
7.1
13.7
3.8
1.0
DNA-PKc
NU7441
7.0
14.7
21.4
18.6
PARP
Olaparib
mCherry
GFP
GFP+ of mCherry+ [%]
100
10
1
0.1
p=0.05
p=0.01
p=0.0004
UTR1
UTR2
neg
3
10
30
0.1
1
10
0.3
1
3
[µM]
controls
Lig1/3
L67
DNA-PKc
NU7441
PARP
Olaparib

Figure 5

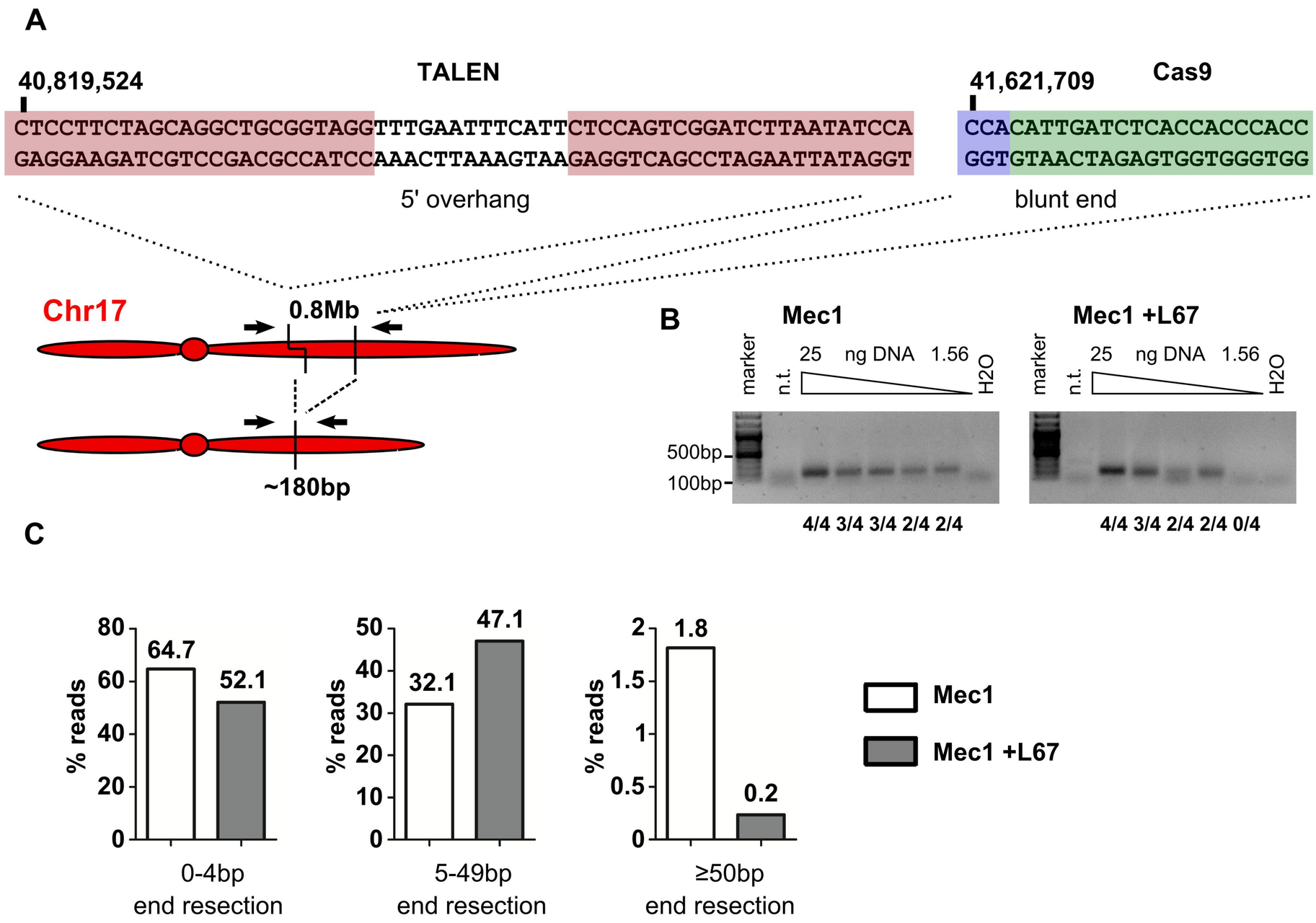
A
40,819,524
TALEN
41,621,709
Cas9
CTCCTTCTAGCAGGCTGCGGTAGGTTTGAATTTCATTCTCCAGTCGGATCTTAATATCCA
GAGGAAGATCGTCCGACGCCATCCAAACTTAAAGTAAGAGGTCAGCCTAGAATTATAGGT
CCACATTGATCTCACCACCCACC
GGTGTAACTAGAGTGGTGGGTGG
5' overhang
blunt end
Chr17
0.8Mb
~180bp
B
Mec1
Mec1 +L67
marker
n.t.
25
ng DNA
1.56
H2O
500bp
100bp
4/4 3/4 3/4 2/4 2/4
4/4 3/4 2/4 2/4 0/4
C
% reads
64.7
52.1
0-4bp
end resection
32.1
47.1
5-49bp
end resection
1.8
0.2
≥50bp
end resection
Mec1
Mec1 +L67

Figure 6